Nitrogen cycling in the Middle Atlantic Bight: Results from a three-dimensional model and implications for the North Atlantic nitrogen budget

Katja Fennel,[1,2] John Wilkin,[1] Julia Levin,[1] John Moisan,[3] John O'Reilly,[4] and Dale Haidvogel[1]

[1]   The biogeochemistry of continental shelf systems plays an important role in the global elemental cycling of nitrogen and carbon, but remains poorly quantified. We have developed a high-resolution physical-biological model for the U.S. east coast continental shelf and adjacent deep ocean that is nested within a basin-wide North Atlantic circulation model in order to estimate nitrogen fluxes in the shelf area of the Middle Atlantic Bight (MAB). Our biological model is a relatively simple representation of nitrogen cycling processes in the water column and organic matter remineralization at the water-sediment interface that explicitly accounts for sediment denitrification. Climatological and regionally integrated means of nitrate, ammonium, and surface chlorophyll are compared with its model equivalents and were found to agree within 1 standard deviation. We also present regional means of primary production and denitrification, and statistical measures of chlorophyll pattern variability. A nitrogen budget for the MAB shows that the sediment denitrification flux is quantitatively important in determining the availability of fixed nitrogen and shelf primary production (it was found to remove 90% of all the nitrogen entering the MAB). Extrapolation of nitrogen fluxes estimated for the MAB to the North Atlantic basin suggests that shelf denitrification removes 2.3×10^{12} mol N annually; this estimate exceeds estimates of N_2 fixation by up to an order of magnitude. Our results emphasize the importance of representing shelf processes in biogeochemical models.

Citation: Fennel, K., J. Wilkin, J. Levin, J. Moisan, J. O'Reilly, and D. Haidvogel (2006), Nitrogen cycling in the Middle Atlantic Bight: Results from a three-dimensional model and implications for the North Atlantic nitrogen budget, *Global Biogeochem. Cycles*, *20*, GB3007, doi:10.1029/2005GB002456.

1. Introduction

[2]   Continental shelves play a key role in the global cycling of biologically essential elements such as nitrogen and carbon. The shelves are known to be highly productive [*Longhurst et al.*, 1995], the majority of the oceanic burial of organic carbon occurs on continental shelves and the adjacent slope [*Premuzic et al.*, 1982; *Hedges and Keil*, 1995], and shelf sediments are important sites for denitrification [*Christensen et al.*, 1987; *Christensen*, 1994]. The loss of fixed nitrogen from the global ocean through denitrification is estimated to exceed the known inputs

[*Codispoti et al.*, 2001, and references therein] and more than half of this removal occurs in sediments, mostly on continental shelves [*Christensen et al.*, 1987]. The exact role of continental shelf processes in global biogeochemical cycling remains, however, poorly quantified. For example, it is still not clear whether the continental shelves presently represent a source or sink of CO_2 to the atmosphere. It has been hypothesized that continental shelves act as a sink for atmospheric CO_2 owing to export of particulate or dissolved organic carbon to the adjacent slope and open ocean [e.g., *Walsh et al.*, 1981; *Smith and MacKenzie*, 1987]. This hypothesis was investigated for the Middle Atlantic Bight (MAB) in the interdisciplinary Shelf Edge Exchange Processes (SEEP) programs I and II [*Walsh et al.*, 1988; *Biscaye et al.*, 1994], which concluded that only a small fraction of particulate carbon (<5%) is exported [*Falkowski et al.*, 1988]. The subsequent Ocean Margins Program (OMP [*Verity et al.*, 2002]) explicitly considered the dissolved and suspended forms of organic carbon in the MAB. OMP results suggest that export of dissolved and suspended organic carbon to the open ocean's interior could be significant provided that advective and eddy diffusive transports are large enough. Another mechanism for the sequestration of inorganic carbon

---

[1]Institute for Marine and Coastal Sciences, Rutgers University, New Brunswick, New Jersey, USA.
[2]Also at Department of Geological Science, Rutgers University, New Brunswick, New Jersey, USA.
[3]Laboratory for Hydrospheric Processes, Observation Science Branch, NASA Goddard Space Flight Center, Wallops Flight Facility, Wallops Island, Virginia, USA.
[4]NOAA National Marine Fisheries Service Narragansett Laboratory, Narragansett, Rhode Island, USA.

could be the winter production of cold, dense shelf water with high inorganic carbon content that is subsequently exported through isopycnal mixing processes [*Tsunogai et al.*, 1999]. This mechanism may represent a globally important carbon flux [*Yool and Fasham*, 2001]. Further investigation and quantification of shelf denitrification in basin-wide and global nitrogen cycling and its potential effect on the carbon balance of shelf systems is also required.

[3] The quantification of elemental exchange fluxes at the ocean margins is in part hindered by their large variability. Exchange processes between the margins and the open ocean occur at mesoscales and within boundary layers, and are highly dynamic. Steady state approximations that are conveniently used for the open oceans (e.g., the concept of new production) are hence problematic. The quantification of biogeochemical processes at the ocean margins will have to rely on a combination of models and observations. In an effort to quantify the elemental fluxes of nitrogen across the shelf boundaries for the MAB, we have constructed a high-resolution, coupled physical-biogeochemical model of the continental shelf of the U.S. east coast and the adjacent deep ocean.

2. Study Area

[4] The Middle Atlantic Bight (MAB) is the region of the eastern continental shelf of the United States that extends from Nantucket Shoals in the north to Cape Hatteras in the south. The hydrography of the region is to a large extent influenced by remote processes: The relatively cool and fresh shelf water entering the bight from the north is part of a larger-scale, coastal current system that can be traced back into the Labrador Sea [*Chapman and Beardsley*, 1989], while in its southern part near Cape Hatteras the influence of the Gulf Stream is immediate with the entrainment of warm and salty waters. The mean circulation is along shelf in the southwestward direction with cross-shelf exchange due to mesoscale processes and transports within the bottom boundary layer. The MAB ecosystem is nitrogen limited, and new nitrogen is supplied by different mechanisms including river and estuarine inputs, upwelling and wind-induced intrusions of slope water and warm-core rings. Chlorophyll concentrations and primary production are highest in the nearshore areas of the MAB adjacent to the mouths of rivers and estuaries and over the shallow water on Georges Bank, and decrease seaward and with increasing water depth. Most of the phytoplankton biomass is made up of nanoplankton (<20 μm), but net plankton (>20 μm; mostly diatoms) can be equally important or more abundant in the nearshore areas of the MAB [*O'Reilly and Zetlin*, 1998]. The seasonal cycle of chlorophyll and primary production is typical of a temperate continental shelf system: a phytoplankton spring bloom during which biomass reaches its annual maximum followed in the summer by lower chlorophyll levels coincident with pronounced stratification, and a secondary bloom in the fall [*O'Reilly et al.*, 1987].

3. Model Description

[5] Our coupled model is comprised of a three-dimensional ocean circulation model, ROMS (Regional Ocean

Modeling System version 2), and a biological model that describes pelagic and benthic aspects of nitrogen cycling. The geographic domain of the physical-biological model extends from the Scotian Shelf to the Gulf of Mexico and includes the adjacent deep ocean. To simulate the influence of circulation processes outside of this domain, such as the subtropical gyre circulation, Gulf Stream mesoscale variability, and inflows from the Gulf of Mexico and Labrador Sea, the coastal model is nested within a high-resolution circulation model for the North Atlantic basin (see auxiliary material[1]).

3.1. Physical Model Configuration

[6] ROMS is a free surface hydrostatic primitive equation ocean model. *Shchepetkin and McWilliams* [2005] describe in detail the algorithms of the ROMS computational kernel. ROMS utilizes a vertically stretched terrain-following coordinate, also called ''s-coordinate,'' that is attractive for the present application because it can be weighted toward the surface to allow enhanced resolution in the model euphotic zone. Here ROMS is implemented for two nested geographic domains: the North Atlantic (NA) basin, and the NorthEast North American (NENA) shelf. Nesting of the NENA domain within the NA model allows us to capture circulation features and variability in the regional domain that is forced in the NA basin. This is done by imposing the NA model's circulation at the open boundaries of the regional model. The NA model's horizontal resolution is 10 km, and 30 sigma levels are used in the vertical direction. Experience has shown that a horizontal resolution near 10 km is necessary to obtain a satisfactory Gulf Stream separation. The circulation model for the NA basin was spun up for 5 years using climatological COADS forcing for heat fluxes and wind forcing, followed by 1 year of spin-up using NCEP reanalysis winds for 1992. The model generates mesoscale variability associated with the Gulf Stream and exhibits seasonal variability due to variable wind forcing in the central NA. The current configuration differs from the one used in the recent DAMEE model intercomparison project for the NA mainly by increased horizontal resolution. In the DAMEE experiments ROMS reproduced many features of the wind-driven and thermohaline circulation and water mass formation [*Haidvogel et al.*, 2000; *Malanotte-Rizzoli et al.*, 2000].

[7] The NENA model has been implemented with similar resolution as in the NA configuration (10 km in the horizontal direction, 30 vertical levels) and is forced with the same 3-day average surface fluxes (this may damp out some higher-frequency variability). A one-way nesting procedure is employed whereby 3-day average temperature, salinity and baroclinic velocity from the basin-wide simulation are imposed at the oceanic perimeter of the shelf model. The depth-average velocity and sea surface height boundary conditions [*Flather*, 1976; *Chapman*, 1985] are used to allow the radiation of gravity waves generated within the domain without upsetting the perimeter tracer fluxes. Coastal freshwater inputs are applied using observed
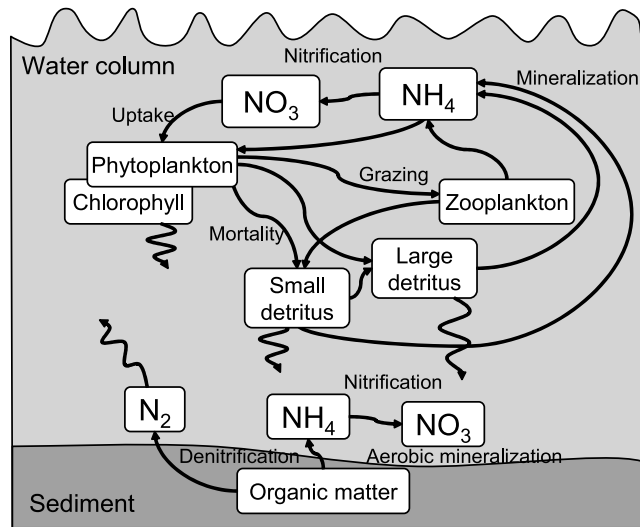

Figure 1. Biological model schematic.

river flow data from USGS and Canadian Rivers. The nesting procedure imposes the NA external variability on the NENA model which exhibits characteristic features of the local and remotely forced circulation, namely, wind-driven upwelling, buoyancy-driven river plumes, lowered salinity on the MAB inner shelf, Gulf Stream intrusions in the South Atlantic Bight, and interactions of Gulf Stream warm rings with the slope waters.

[8] Tidal currents and the associated mixing are relatively small in most of our model domain, including the MAB, except for the Gulf of Maine/Bay of Fundy system [*Moody et al.*, 1984]. The Gulf of Maine responds in a nearly resonant fashion to the forcing of deep ocean tides at the edge of the shelf resulting in growing amplitudes of the M_2 tide (the dominant tidal component) from 0.5 m at the seaward side of Georges Bank to 4 m in the Bay of Fundy and exceeding 6 m in its easternmost extension [*Garrett*, 1972; *Moody et al.*, 1984; *Lynch and Naimie*, 1993]. The required large tidal transports flowing over the shallow Georges Bank result in tidal currents of 80–100 cm/s over Georges Bank and strong dissipative mixing, neither of which are found in the western Gulf of Maine or the New England shelf [*Brown*, 1984]. Because the focus of this study is the MAB we choose to neglect tides in favor of increased computational efficiency (the inclusion of tidal currents would require a significantly reduced model time step).

3.2. Biological Model Component

[9] Our biological model is a representation of the pelagic nitrogen cycle and includes seven state variables: phytoplankton, *Phy*, zooplankton, *Zoo*, nitrate, *NO3*, ammonium, *NH4*, small and large detritus, *SDet* and *LDet*, and phytoplankton chlorophyll, *Chl*, (Figure 1). Since our model's basic structure follows the widely applied Fasham model [*Fasham et al.*, 1990], we mainly focus on our modifications of the Fasham model in the following description.

[10] The time rate of change of phytoplankton due to biological sources and sinks is given by

$$\frac{\partial Phy}{\partial t} = \mu Phy - gZoo - m_P Phy - \tau(SDet + Phy)Phy - w_P\frac{\partial Phy}{\partial z} \quad (1)$$

The growth rate of phytoplankton, μ, depends on the temperature T through the maximum growth rate $\mu_{max} = \mu_{max}(T) = \mu_0 \cdot 1.066^T$ [*Eppley*, 1972], on the photosynthetically available radiation I, and on the nutrient concentrations *NO3* and *NH4*,

$$\mu = \mu_{max} \cdot f(I) \cdot (L_{NO3} + L_{NH4}), \quad (2)$$

where

$$L_{NO3} = \frac{NO3}{k_{NO3} + NO3} \cdot \frac{1}{1 + NH4/k_{NH4}} \quad (3)$$

$$L_{NH4} = \frac{NH4}{k_{NH4} + NH4}. \quad (4)$$

I is exponentially decreasing with water depth z according to

$$I = I(z) = I_0 \cdot par \cdot \exp\left\{-z\left(K_w + K_{chl}\int_z^0 Ch(\zeta)d\zeta\right)\right\}, \quad (5)$$

where I_0 is the incoming light just below the sea surface, and *par* is the fraction of light that is available for photosynthesis and equals 0.43. I_0 is the shortwave radiation flux from the NCEP reanalysis data set, but modulated depending on local latitude, longitude and day-of-the-year to provide the local diurnal cycle. K_w and K_{chl} are the light attenuation coefficients for water and chlorophyll, respectively, and are set to 0.04 m^{-1} and 0.025 (mg Chl)$^{-1}$ m^{-2} [*Kirk*, 1983]. The function $f(I)$ represents the photosynthesis-light (P-I) relationship [*Evans and Parslow*, 1985],

$$f(I) = \frac{\alpha I}{\sqrt{\mu_{max}^2 + \alpha^2 I^2}}, \quad (6)$$

where α is the initial slope. Nutrient limitation is represented by the sum of Michealis-Menten functions for nitrate and ammonium, L_{NO3} and L_{NH4}, and nitrate uptake is assumed to be inhibited in the presence of ammonium through the factor $1/(1 + NH4/k_{NH4})$ following *Parker* [1993]. (We chose not to use the exponential ammonium inhibition term used by *Fasham et al.* [1990] because this parameterization has two undesirable features, namely the nitrogen uptake rate does not increase monotonically with increasing ammonium concentrations for nitrate concentrations above about 1 mmol N m^{-3} and the expression is not limited to values of less than or equal to 1 and hence can not be treated as a nondimensional limitation term (see R. R. Hood and J. R. Christian (N-cycle modeling, submitted to *Nitrogen in the*

Marine Environment, edited by E. J. Carpenter and D. G. Capone, Elsevier, 2006) for a discussion).) Here k_{NO3} and k_{NH4} are the half-saturation concentrations for uptake of nitrate and ammonium, respectively.

[11] The rate of phytoplankton grazing, g, by zooplankton is represented by a Holling-type s-shaped curve as

$$g = g_{\max} \frac{Phy^2}{k_P + Phy^2}, \tag{7}$$

with $g_{\max}$ as maximum grazing rate and k_P as half-saturation concentration for phytoplankton ingestion. (The Holling-type III or s-shaped grazing response is commonly used in models, has been fit to experimental data, and is known to be numerically more stable than the linear response which can give rise to large-amplitude limit cycles [see *Gentleman et al.*, 2003, and references therein].) Other phytoplankton loss terms are mortality, represented by the linear rate m_P, aggregation of phytoplankton and small detritus to large detritus, and vertical sinking. We allow small detrital particles (*SDet;* particles smaller than 10 μm) and phytoplankton (*Phy*) to aggregate and form larger detrital particles (*LDet*). The aggregation rate is assumed to scale with the square of small particle abundance (*SDet*+*Phy*) because particle encounter rates increase for higher particle abundances, and is multiplied by the aggregation factor τ. w_P is a constant vertical sinking velocity.

[12] The relationship between chlorophyll and phytoplankton biomass is nonlinear, because the chlorophyll content per phytoplankton cell changes as the cell's photosynthetic apparatus acclimates to changes in light and nutrient conditions [*Falkowski*, 1980; *Laws and Bannister*, 1980; *Sakshaug et al.*, 1989]. We account for the effects of this photoacclimation on the basis of the model of *Geider et al.* [1996, 1997]. The dynamics of chlorophyll is derived from the phytoplankton equation by conversion into chlorophyll units, i.e., by multiplication with the ratio of chlorophyll to phytoplankton biomass and the assumption that only a fraction of phytoplankton growth is devoted to chlorophyll synthesis. This fraction, ρ_{chl}, is defined as

$$\rho_{chl} = \frac{\theta_{\max} \mu Phy}{\alpha IChl}, \tag{8}$$

where $\theta_{\max}$ is the maximum ratio of chlorophyll to phytoplankton biomass. Here ρ_{chl} is regulated by the ratio of achieved-to-maximum potential photosynthesis (μPhy)/($\alpha ICHL$) [*Geider et al.*, 1997]. The time rate of change of chlorophyll follows as

$$\frac{\partial Chl}{\partial t} = \rho_{Chl}\mu Chl - gZoo\frac{Chl}{Phy} - m_P Chl - \tau(SDet + Phy)Chl. \tag{9}$$

Zooplankton is assumed to assimilate ingested phytoplankton with the efficiency β while the remaining fraction is being transferred to the small detritus pool. Other zooplankton loss terms are excretion and mortality. Excretion to ammonium is comprised of excretion due to basal metabolism at the linear rate l_{BM} and an assimilation-dependent excretion that is proportional to the assimilation

of ingested phytoplankton and has the maximum rate l_E. Zooplankton mortality is assumed to scale with the square of zooplankton biomass and is transferred into the pool of small detritus. The time rates of change of zooplankton and the detrital pools follow as

$$\frac{\partial Zoo}{\partial t} = g\beta Zoo - l_{BM}Zoo - l_E \frac{Phy^2}{k_P + Phy^2}\beta Zoo - m_Z Zoo^2 \tag{10}$$

$$\frac{\partial SDet}{\partial t} = g(1-\beta)Zoo + m_Z Zoo^2 + m_P Phy - \tau(SDet + Phy)SDet$$
$$- r_{SD}SDet - w_S\frac{\partial SDet}{\partial z} \tag{11}$$

$$\frac{\partial LDet}{\partial t} = \tau(SDet + Phy)^2 - r_{LD}LDet - w_L\frac{\partial LDet}{\partial z}. \tag{12}$$

Here r_{SD} and r_{LD} are the remineralization rates for the small and large detritus pools, respectively, and w_S and w_L are their respective sinking velocities.

[13] Detritus remineralization feeds into the ammonium pool, and ammonium is subsequently nitrified to produce nitrate. The nitrification rate n is described by $n = n_{\max}\left(1 - \max\left[0, \frac{I - I_0}{k_I + I - I_0}\right]\right)$, where $n_{\max}$ is the maximum rate of nitrification. Since nitrification is inhibited by light and the level of minimum inhibition is reached at nonzero light intensities [*Olson*, 1981], it is assumed to drop off to zero at high light intensities with k_I as the light intensity at which inhibition is half-saturated and an inhibition threshold of I_0.

[14] The time rates of change due to biological processes for nitrate and ammonium are

$$\frac{\partial NO3}{\partial t} = -\mu_{\max}f(I)L_{NO3}Phy + nNH4 \tag{13}$$

$$\frac{\partial NH4}{\partial t} = -\mu_{\max}f(I)L_{NH4}Phy - nNH4 + l_{BM}Zoo$$
$$+ l_E\frac{Phy^2}{k_P + Phy^2}\beta \cdot Zoo + r_{SD}SDet + r_{LD}LDet. \tag{14}$$

Note that the bottom boundary condition (equation (15)) will result in an additional source of ammonium in the bottom layer. Values for the model parameters are listed in Table 1 in comparison with parameter values from the literature.

3.3. Sediment Processes

[15] A significant fraction of the organic matter entering estuarine and coastal systems (through primary production or import) is mineralized by the benthos, and only a small fraction is permanently buried [*Nixon and Pilson*, 1983]. Most of the nitrogen associated with the organic matter reaching the bottom is returned rapidly to the overlying water in the form of ammonium, although the rate of this process is markedly dependent on temperature [*Nixon et al.*, 1976; *Aller*, 1980]. The sediment component of our model

Table 1. Biological Model Parameters Used in This Study and Range of Published Parameter Values

Symbol	Parameter	Value	Unit	Range
μ_0	phytoplankton growth rate at 0°C	0.69	d^{-1}	$0.62^a-3.0^{b,c}$
k_{NO3}	half-saturation concentration for uptake of NO_3	0.5	mmol N m^{-3}	$0.007-1.5^d$
k_{NH4}	half-saturation concentration for uptake of NH_4	0.5	mmol N m^{-3}	$0.007-1.5^d$
α	initial slope of the P-I curve	0.125	molC $gChl^{-1}$ $(W\ m^{-2})^{-1}$ d^{-1}	$0.007-0.13^e$
g_{max}	maximum grazing rate	0.6	$(mmol\ N\ m^{-3})^{-1}$ d^{-1}	$0.5^f-1.0^g$
k_P	half-saturation concentration of phytoplankton ingestion	2	$(mmol\ N\ m^{-3})^2$	$0.56-3.5^{d,h}$
m_P	phytoplankton mortality	0.15	d^{-1}	$0.05-0.2^i$
τ	aggregation parameter	0.005	$(mmol\ N\ m^{-3})^{-1}$ d^{-1}	0.1^d
Θ_{max}	maximum chlorophyll to phytoplankton ratio	0.053	mgChl mgC^{-1}	$0.005-0.072^e$
β	assimilation efficiency	0.75	dimensionless	see references^{j,k}
l_{BM}	excretion rate due to basal metabolism	0.1	d^{-1}	see references^j
l_E	maximum rate of assimilation related excretion	0.1	d^{-1}	see references^j
m_Z	zooplankton mortality	0.025	$(mmol\ N\ m^{-3})^{-1}$ d^{-1}	$0.05^l-0.25^d$
r_{SD}	remineralization rate of suspended detritus	0.03	d^{-1}	$0.01-0.25^j$
r_{LD}	remineralization rate of large detritus	0.01	d^{-1}	$0.01-0.25^j$
n_{max}	maximum nitrification rate	0.05	d^{-1}	0.1^d
k_I	light intensity at which the inhibition of nitrification is half-saturated	0.1	W m^{-2}	see references^{m,n}
I_0	threshold for light-inhibition of nitrification	0.0095	W m^{-2}	see references^{m,n}
w_{Phy}	sinking velocity of phytoplankton	0.1	m d^{-1}	0.009^o-25^d
w_{SDet}	sinking velocity of suspended detritus	0.1	m d^{-1}	0.009^o-25^d
w_{LDet}	sinking velocity of larger particles	1	m d^{-1}	0.009^o-25^d

[a]*Taylor* [1988].
[b]*Andersen et al.* [1987].
[c]Note that owing to the temperature dependence for a temperature range from 0° to 20°C the maximum growth rate in our model varies from 0.69 to 2.49 d^{-1}.
[d]*Lima and Doney* [2004].
[e]*Geider et al.* [1997].
[f]*Wroblewski* [1989].
[g]*Fasham* [1995].
[h]Note that the values were squared to be consistent with the notation our model.
[i]*Taylor et al.* [1991].
[j]*Leonard et al.* [1999].
[k]*Oschlies and Garcon* [1999].
[l]*Fennel et al.* [2001].
[m]*Olson* [1981].
[n]Note that Olson differentiates between the oxidation of ammonium to nitrite and nitrite to nitrate.
[o]*Moskilde* [1996].

is a simple representation of benthic mineralization processes; that is, the remineralization of deposited organic matter in the upper part of the sediment is formulated as a bottom boundary condition. This implies that the flux of sinking organic matter out of the bottommost grid box results immediately in a corresponding influx of inorganic nutrients at the sediment/water interface. In the classification of benthic-pelagic coupling formulations by *Soetaert et al.* [2000], this approach is considered of intermediate complexity (a mass conserving formulation that assumes immediate equilibrium between particle deposition and the return flux of dissolved constituents from the sediment). *Soetaert et al.* [2000] showed that this computationally efficient approach captures most of the dynamics inherent in benthic-pelagic coupling. Consideration of a delayed coupling, i.e., the accumulation of deposited organic matter coupled to a temperature-dependent decomposition, would require a computationally more expensive diagenetic model.

[16] Continental shelf sediments are essentially anaerobic environments except for a thin oxygenated layer beneath the water/sediment interface and around animal burrows. Both aerobic and anaerobic mineralization are thus important pathways of carbon oxidation, but have a different yield of dissolved inorganic nitrogen. Degradation of organic matter in the anaerobic sediment is carried out by various bacteria which use a range of redox reactions and different

electron acceptors. These different metabolic types each exploit only a fraction of the organic matter's energy and are ordered vertically according to their decreasing redox potential and energy yield [*Jørgensen*, 1996]. Aerobic respiration occurs in the upper few millimeters of the sediment, where oxygen is present, followed by denitrification (nitrate respiration), manganese and iron reduction (in the brown oxidized sediment from a few millimeters to 10 cm deep), sulfate reduction (down to several meters), and methanogenesis, the terminal metabolism for organic matter oxidation after depletion of all other oxidants [*Jørgensen*, 1996]. Here we assume that coupled nitrification-denitrification is the dominant aerobic mineralization pathway as has been found by *Laursen and Seitzinger* [2002] in MAB sediments off the New Jersey coast, although sulfate reduction can be a significant fraction of organic matter respiration especially in organic rich, muddy sediments [*Mackin and Swider*, 1989].

[17] We account for the aerobic and anaerobic pathways, assuming that the fraction of carbon oxidation that occurs through each mineralization route is fixed. *Seitzinger and Giblin* [1996] compiled available denitrification rates for continental shelves and found a robust linear relationship between sediment oxygen consumption and denitrification. They focused on the portion of denitrification that is based on nitrate derived from the nitrification of ammonium in the

sediment, also referred to as coupled nitrification/denitrification. Direct denitrification in contrast relies on nitrate from overlying water that diffuses into the sediment or is transported by macrofauna irrigation. There are conflicting reports about the importance of direct denitrification. Shelf sites where nitrate uptake by the sediment from the overlying bottom water has been found to be unimportant compared to coupled nitrification/denitrification include the LEO site in the MAB [*Laursen and Seitzinger*, 2002], the South Atlantic Bight [*Hopkinson et al.*, 1991], the shallow Long Island Sound [*Mackin and Swider*, 1989], North Sea sediments [*Raaphorst et al.*, 1990; *Lohse et al.*, 1993], and Boston Harbor [*Kelly and Nowicki*, 1993; *Giblin et al.*, 1994]. Sites where direct denitrification has been found to be similar to or greater than coupled nitrification/denitrification include the Washington Shelf and the Gulf of Maine [*Christensen et al.*, 1987; *Devol*, 1991; *Devol and Christensen*, 1993], the Baltic Sea [*Jensen et al.*, 1990], and off Cap Blanc, Africa [*Rowe et al.*, 1977]. In principle, direct denitrification should vary with the bottom water nitrate concentration, but to the best of our knowledge, no quantitative model like the one for coupled nitrification/denitrification by *Seitzinger and Giblin* [1996] presently exists. We use the linear relationship between sediment oxygen consumption and denitrification by *Seitzinger and Giblin* [1996] which will underestimate the removal of fixed nitrogen from systems where direct denitrification is quantitatively important.

[18] With regard to sulfate reduction, *Mackin and Swider* [1989] found this process to contribute 65–85% of organic matter decomposition on a shallow site in Long Island Sound. They measured no nitrate in pore waters and no flux of ammonium from the sediment into the overlying water, indicating that remineralized ammonium is completely oxidized before it escapes across the sediment water interface through a combination of nitrification and sulfide oxidation. However, assuming that sulfate reduction coupled with nitrification and sulfide oxidation is the dominant pathway of organic matter oxidation instead of coupled nitrification-denitrification does not significantly affect our assumption about the influx of fixed nitrogen at the sediment/water interface (see Appendix A). Consequently sediment remineralization should be described reasonably well by assuming a constant fraction of denitrification to total mineralization based on the linear relationship between sediment oxygen consumption and denitrification by *Seitzinger and Giblin* [1996].

[19] *Seitzinger and Giblin*'s [1996] relationship quantitatively relates the oxygen uptake of the sediment to an efflux of N_2. In order to determine the sediment efflux of fixed nitrogen (ammonium) we assume that the sediment consumption of oxygen is related to carbon oxidation; in other words, oxygen is consumed either in the oxidation of organic matter or in the nitrification of ammonium to nitrate which is then used in denitrification. Since aerobic mineralization, nitrification and denitrification occur according to known stoichiometries we can determine which fraction of organic matter mineralization occurs through denitrification. Our calculation (given in detail in Appendix A) results in a denitrification fraction of 14% and an oxygenic mineraliza-

tion fraction of 86%. It follows that the oxidation of one mole of organic matter (containing 16 moles of nitrogen) yields 4 moles of ammonium, while 6 moles of N_2 are denitrified and lost from the pool of bioavailable fixed nitrogen. Our bottom boundary condition hence reads

$$\frac{\partial}{\partial t}NH4\bigg|_{z=H} = \frac{4}{16\Delta z}\left(w_{Phy}Phy|_{z=H} + w_{SDet}SDet|_{z=H} + w_{LDet}LDet|_{z=H}\right),$$
(15)

where Δz is the thickness of the bottom model layer.

3.4. Initial and Boundary Conditions

[20] Initial and boundary conditions for nitrate were derived using polynomial approximations that predict nitrate concentrations as function of temperature and were derived from the NODC World Ocean Database 2001 (see auxiliary material). As this relationship differs between shelf water and slope/open ocean waters, two different approximations were used for the shelf (defined as the area with water depths shallower than 250 m) and the slope/open ocean. All other biological variables were set initially to a homogeneous, small value of 0.1 mmol N m^{-3}. Experience has shown this approach to work well, because the adjustment timescales for these variables are short (on the order of days to weeks). Since the biological component of our model is only implemented in the coastal (NENA) domain, open boundary concentrations for the biological state variables have to be prescribed without reference to an outer domain model. We used the same procedure for prescribing the boundary concentrations as for the initial conditions. Consequently, phytoplankton and zooplankton concentrations in water entering the domain are low, and some bogus primary productivity near the open boundaries can result as variables adjust to values more typical of the inner domain. However, this boundary artifact occurs only in the close vicinity of inflow boundaries and does not affect the area of the MAB. River concentrations of nitrate, ammonium and organic nitrogen (PON and DON where available) from the U.S. Geological Survey monitoring database were used to derive a monthly climatology of these conditions and subsequently multiplied with the freshwater flux to yield the river inputs of nutrients and PON (see J. Moisan and A. Mason, manuscript in preparation, 2006, for details).

4. Results

[21] The coastal biogeochemical model was initialized with the state of the NA model at 1 January 1993, spun up for 1 year, and integrated for the subsequent 2 years (1994 and 1995). This simulation is evaluated in the following subsection with particular focus on the MAB.

4.1. Model/Data Comparison

[22] Available data sets for a model/data comparison in the MAB include (1) biochemical in situ data from the OMP in 1994 [*Verity et al.*, 2002], the SEEP experiments in 1983–1984 and 1988–1989 [*Walsh et al.*, 1988; *Biscaye et al.*, 1994], and a number of cruises undertaken by Brookhaven National Laboratory between 1974 and 1995
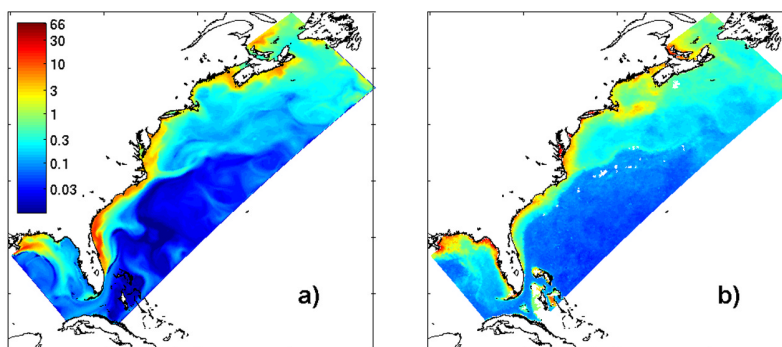
Figure 2. (a) Model-simulated mean surface chlorophyll for July of 1994 and (b) SeaWiFS mean chlorophyll for July of 2003 (same colorscale).

(BNL data reports); (2) in situ data of primary production from the MARMAP cruises [*O'Reilly and Zetlin*, 1998]; and (3) remotely sensed surface chlorophyll data from the SeaWiFS sensor and primary productivity estimates derived from SeaWiFS data from January 1998 through December 2004. The biochemical variables in the in situ data set, which were merged from the above-mentioned sources, include chlorophyll, nitrate and ammonium concentrations. A monthly climatology of these variables for the inner and outer shelf (delineated by the 50-m isobath) was generated for model/data comparison. The 9-km resolution SeaWiFS Standard Mapped Images data are available from 1998 to 2004. Monthly mean fields and a monthly climatology have been generated from this data set. Remotely sensed estimates of surface chlorophyll concentration and photosynthetically active radiation (PAR) from SeaWiFS and sea surface temperature (SST) from the NOAA AVHRR sensor were used with the Vertically Generalized Productivity Model (VGPM [*Behrenfeld and Falkowski*, 1997]) to estimate primary production. In the VGPM, the optimal rate of productivity (P_b^{opt}: optimal water column carbon fixation (mg C (mg chlorophyll a)$^{-1}$ h^{-1}) is modeled as a seventh-order polynomial function of SST. In our application of the VGPM, which we designate as VGPM2, the relationship between P_b^{opt} and SST follows the exponential relationship by *Eppley* [1972], as modified by *Antoine et al.* [1996]. A trial of the VGPM, VGPM2 and three other productivity models revealed that the VGPM2 yielded the best agreement (smallest RMS error) with the MARMAP seasonal productivity cycle for the northeast shelf ecosystem.

[23] An example of spatial patterns in surface chlorophyll is given in Figure 2, where the simulated mean surface chlorophyll for July 1994 is shown in comparison to the SeaWiFS chlorophyll for July 2003 (note that SeaWiFS data is not available for 1994). Chlorophyll concentrations are highest near the coast, decrease on the outer shelf and again in the slope waters with local chlorophyll maxima in the Gulf Stream front; lowest concentrations are found in the Sargasso Sea. The model underestimates surface chlorophyll on Georges Bank when compared to SeaWiFS chlorophyll.

[24] For a more thorough assessment of model/data agreement we now present statistical measures to quantify the overall correspondence between observed and simulated surface nitrate, ammonium and chlorophyll. First, we com-

pare regional means and variances of simulated and in situ nitrate and ammonium, and simulated, in situ and SeaWiFS surface chlorophyll. Statistical measures of chlorophyll pattern agreement (with the overall bias removed) will be given below. The temporal evolution of surface nitrate and ammonium (upper 20 m) is compared to its model equivalents for the inner and outer shelf of the MAB in Figure 3. The simulated nitrate concentrations overestimate the observed values in winter and spring, while the simulated ammonium concentrations underestimate the observed values, possibly because the model nitrifies ammonium too efficiently on the inner shelf. However, the simulated and observed nutrient concentrations agree within one standard deviation except for one instance in February on the outer shelf.

[25] The temporal evolution of monthly mean surface chlorophyll from the in situ and SeaWiFS climatologies and the model are shown in Figure 4 for the inner and outer shelf of the MAB, the adjacent slope and Georges Bank. There is a notable difference between the inner shelf and the outer shelf and slope regions with higher mean chlorophyll
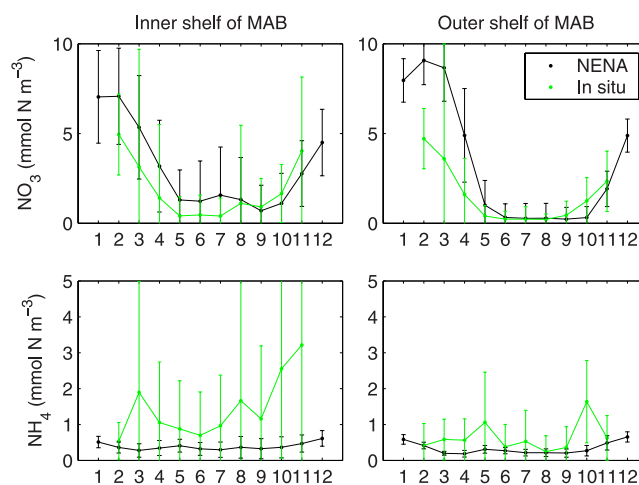

Figure 3. Monthly means and standard deviations of surface (upper 20 m) nitrate and ammonium concentrations on the inner and outer shelf of the Middle Atlantic Bight as predicted by the NENA model and an in situ climatology (see text for details on data sources).
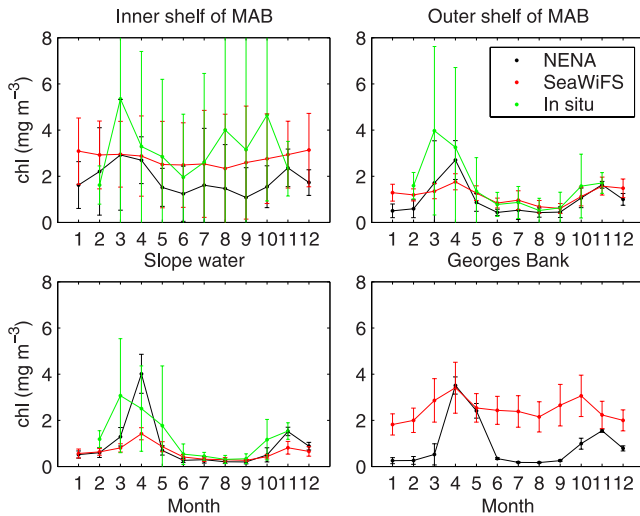
Figure 4. Monthly means and standard deviations of surface chlorophyll on the inner and outer shelf of the MAB, in the adjacent slope region, and on Georges Bank as predicted by the NENA model and SeaWiFS and in situ climatologies (see text for details on data sources).

levels and higher variances throughout the year and no pronounced seasonal cycle on the inner shelf. On the outer shelf and in the slope water both in situ and model data show a pronounced peak in surface chlorophyll in the spring and a smaller peak in the fall. There are no statistically significant differences between the model and data in the inner shelf, outer shelf, and slope water regions; however, the model consistently underestimates SeaWiFS chlorophyll on Georges Bank. This discrepancy is likely due to the lack of tides in the current implementation of our physical model. Tidal mixing is thought to be the main mechanism of nutrient supply on Georges Bank supporting the high levels of productivity observed there [*Chen and Beardsley*, 1998]. Regional models of the Gulf of Maine that include tidal forcing show more realistic levels of chlorophyll and productivity on Georges Bank [*Franks and Chen*, 1996]. Comparisons of observed and simulated tidal amplitudes and associated mixing show that tidal effects are significantly smaller on the New England shelf (the northern tip of the MAB) than on Georges Bank [*Moody et al.*, 1984; *Brown*, 1984]. Evidence for even smaller tidal effects southwest of the New England shelf comes from indices of vertical stratification [e.g., *O'Reilly and Zetlin*, 1998; Figures 29 and 30; *Falkowski et al.*, 1988], which indicate that the MAB is among the most strongly stratified regions in the world.

[26] In addition to agreement in the mean course of simulated and observed variables shown in Figures 3 and 4 we expect correspondence between patterns of simulated and observed variability. Statistical measures commonly used to compare a model-simulated field, or "test field," with an observed field, or "reference field," with regard to pattern correspondence are the standard deviations of the two fields, the correlation between the two fields, and the pattern root-mean squared (RMS) difference between the fields. The standard deviations measure the amplitude of

variations in the respective field, the correlation coefficient measures the agreement in the pattern of variation between the two fields regardless of the amplitude, and the centered RMS difference measures the differences between the two fields with the overall bias removed; the three provide complementary statistical information. The ratio of the standard deviations of the two fields, their correlation, and their centered RMS difference can be displayed by one point in a 2D diagram (Taylor diagram [*Taylor*, 2001]), which is particularly useful when more than one set of fields is compared. A brief explanation of the diagram is given in Appendix B.

[27] To assess pattern correspondence, the SeaWiFS data was interpolated onto the model grid and log-transformed, since the SeaWiFS and model surface chlorophyll data are lognormally distributed. We follow *Lima and Doney* [2004] in considering two statistics (total time–space and spatial-annual) and calculated these for the whole domain and the MAB area only. The total time-space statistic measures temporal and spatial variations around the total mean. The spatial-annual statistic measures spatial variations of the annual mean around the total mean.

[28] The measures of pattern correspondence of each individual SeaWiFS year with the monthly SeaWiFS climatology are given in Figure 5. The ensemble of SeaWiFS points in Figure 5 illustrates the discrepancies to be expected when comparing a single year to the climatology. Note that model results are expected to deviate somewhat from the climatology owing to unresolved internal variability, imperfect initial and forcing conditions, and most importantly in our case owing to interannual variability. Hence apparent differences between the test and the reference fields may be statistically or practically insignificant. The expected level of difference in pattern correspondence due to interannual variability can be gauged by the comparison of the individual SeaWiFS years (1998–2004) with the climatology. If the whole domain is considered, the match between an individual SeaWiFS year and the climatology is within 10% of the amplitudes of variations ($0.9 \leq \sigma_n \leq 1.1$), with a correlation $R > 0.9$, and an RMS difference $E < 0.4$. With the exception of 1998, a similar match is obtained when the analysis is restricted to the MAB. 1998 is anomalous with amplitudes of variation significantly larger than the climatology and the other SeaWiFS years. In 1998, mean chlorophyll levels were smaller during summer but their variance was larger throughout the year. The patterns of modeled surface chlorophyll and the SeaWiFS climatology are within 40% of the amplitudes of variation ($0.6 \leq \sigma_n \leq 1.4$) and have a lower correlation ($\sim 0.4 – \sim 0.8$). The model's spatial resolution is thus sufficient to capture the variability of surface chlorophyll that is represented by the 9-km SeaWiFS data. In fact, when the statistics are restricted to the MAB the simulated patterns match the SeaWiFS climatology more closely in terms of centered RMS difference and correlation than SeaWiFS 1998.

4.2. Model/Data Comparison: Fluxes

[29] Model-simulated primary productivity is highest on the inner shelf of the MAB and the South Atlantic Bight

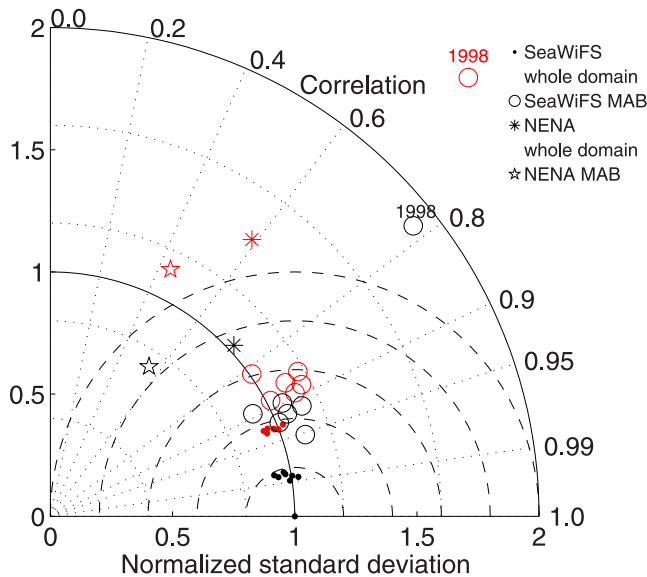**Figure 5.** Taylor diagram comparing monthly mean fields of log-transformed chlorophyll estimates from the model and SeaWiFS (the "test" fields) with a log-transformed SeaWiFS climatology (the "reference" field indicated by the black dot on the *x* axis) for the whole model domain and for the Middle Atlantic Bight only. The radial distances from the origin are proportional to the ratio standard deviations; the azimuthal positions indicate the correlation coefficient; and the distance between the "test" points and the "reference" point indicates the centered RMS difference. The definitions of the total time-space (red) and spatial-annual (black) statistics are given in Appendix B.

(extending from Cape Hatteras to the southern tip of Florida), and lowest in the oligotrophic Sargasso Sea (see auxiliary material). The shallow water depth on the shelf enables efficient nutrient recycling due to the pronounced benthic-pelagic coupling which contributes to the high primary productivity. The simulated primary productivity for the MAB (the shelf area shallower than 100 m between Nantucket Shoals and Cape Hatteras) is 200 g C m^{-2} yr^{-1}, lower than the observational estimates of 310 g C m^{-2} yr^{-1} for the MAB [*O'Reilly and Busch*, 1984] and 290 g C m^{-2} yr^{-1} for the New York Bight [*Malone et al.*, 1983].

[30] The annual productivity illustrates that boundary effects in the biological model component are small. While chlorophyll levels can be elevated near the open boundaries at times (see, for example, the northern boundary in Figure 2), annual mean production is elevated owing to boundary artifacts only at the northern boundary on the Labrador Shelf. The area of elevated production is localized in the vicinity of the boundary, and does not affect the shelf region of the MAB which is the primary focus of this study.

[31] A comparison of monthly means and variances of model-predicted, satellite-derived and in situ primary production is given in Figure 6 for the inner and outer shelf of the MAB, the adjacent slope and Georges Bank. On the inner shelf the model consistently underestimates both satellite and in situ primary production, although the

model-predicted values are within 1 standard deviation of the in situ climatology. The satellite-derived primary production overestimates in situ primary production on the inner shelf, although satellite-derived chlorophyll is slightly underestimating the in situ chlorophyll (Figure 4). This illustrates that the primary productivity algorithms may be problematic for the optically complex nearshore region. On the outer shelf and over the adjacent slope the model underestimates in situ and VGPM2 primary production, but the mean values are within 1 standard deviation of each other. However, the discrepancy is more pronounced on Georges Bank as we would expect. The satellite-derived and in situ primary production estimates appear to agree well on the outer shelf, in the slope water and on Georges Bank.

[32] The annual denitrification flux for the MAB is largest in the estuaries, Chesapeake Bay and Delaware Bay, and on the inner shelf above the 50-m isobath. The mean annual flux for the MAB is 1.1 mmol N m^{-2} d^{-1} and compares well with the extrapolations of *Seitzinger and Giblin* [1996], who estimated a mean flux of 0.7 mmol N m^{-2} d^{-1} for the shelf area of the entire NA and a mean flux of 1.4 mmol N m^{-2} d^{-1} for the shelf area between Nova Scotia and Cape Hatteras. Direct measurements of sediment denitrification at the LEO-15 site located at 39°28′N, 74°15′W on the inner shelf of the MAB are similar with a mean flux of 1.7 ± 0.6 mmol N m^{-2} d^{-1} [*Laursen and Seitzinger*, 2002]. We conducted a sensitivity study in order to assess how the predicted denitrification flux depends on the assumed sinking velocity of organic matter which is generally a poorly constrained parameter. Given the computational cost of the coupled simulations in the full domain we chose to vary the sinking velocity in a quasi-1D framework (a 5 × 5 grid point domain with double-periodic boundary conditions and otherwise identical set-up to the full 3D model). We varied the water depth from 210 m to 25 m and changed the sinking velocity of organic matter by ±50%. The annual
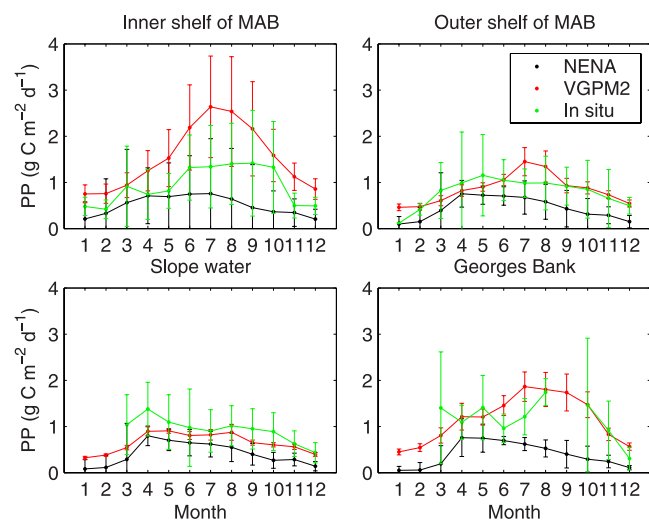

Figure 6. Monthly means and standard deviations of primary production from the NENA model, VGPM2 and an in situ climatology derived from the MARMAP data set.
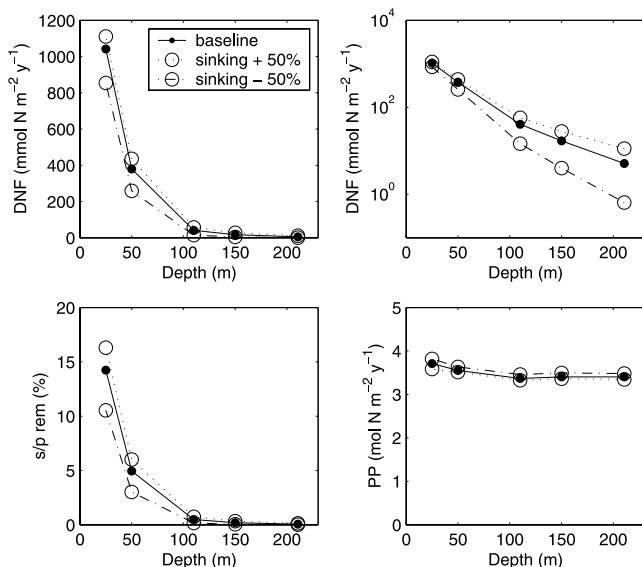
Figure 7. Results of a sensitivity study in a quasi-one-dimensional ROMS framework. The simulated annual sediment denitrification flux (DNF), primary production (PP) and the ratio of sediment to pelagic remineralization (s/p rem) are shown for five different water depths and for the default sinking velocity (solid symbols; see Table 1 for sinking parameters) as well as for sinking velocities ±50% of the default values (open circles).

denitrification flux, primary production and the ratio of sediment to pelagic remineralization are shown in Figure 7. While the primary production is essentially independent of water depth and sinking velocity, the sediment denitrification flux increases exponentially with decreasing water depth. Faster sinking of organic matter slightly increases sediment remineralization and slightly decreases primary production, as one would expect, but the dependence of the denitrification flux on water depth appears to be dominant. This dependence is a direct consequence of the exponentially increasing fraction of organic matter oxidation in the sediment with decreasing water depth. Observational evidence in support of this
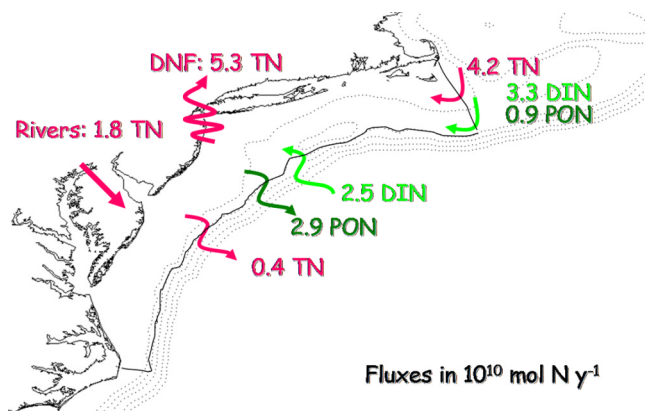
exponential dependence comes from the biomass of benthic suspension feeders: It also increases exponentially with decreasing water depth [*Middelburg and Soetaert*, 2004].

4.3. Nitrogen Budget for the MAB

[33] We derived a nitrogen budget for the MAB by diagnosing the model-simulated fluxes of particulate and dissolved nitrogen across the MAB boundaries (across two cross-shelf transects near Nantucket Shoals and Cape Hatteras and across the 100-m isobath) as well as river inputs and losses due to denitrification (Figure 8). Total nitrogen (TN = DIN + PON) enters the MAB from the north and from rivers, but the import from the north is more than double the river input. Denitrification removes 90% of TN entering the MAB, while the rest is exported across the shelf break. Interestingly, while the mean volume transport across the shelf break is out of the MAB and accompanied by an export of particulate nitrogen (PON), there is a significant cross-isobath inflow of nitrate, illustrating that hydrographic characteristics do not constrain tracer fluxes per se. The denitrification loss is significantly larger than the river input of nitrogen, making the shelves of the MAB a net sink of fixed nitrogen.

5. Discussion and Conclusions

[34] The high spatial resolution necessary to capture the small-scale features of margin topography, as well as mesoscale and small-scale currents and the resulting fluxes of nutrients and organic matter represent a challenge to resolving biogeochemical processes at ocean margins. In our approach a high-resolution coupled model of the continental shelves is nested within a larger-scale circulation model of the NA. In the nesting procedure open boundary information for currents, temperature and salinity is provided from the large-scale circulation model to the regional model, but boundary information for the biochemical variables has to be prescribed. We used a simple approach to prescribing the biochemical variables where nitrate concentrations are determined from temperature using approximations that were derived from the NODC data set, and all other variables

Figure 8. Nitrogen budget for the MAB.

Table 2. North Atlantic Flux Estimates

Data Source	Estimate
N Sink: Sediment Denitrification, mol N yr⁻¹	
Model (this study)	2.3×10^{12}
	(MAB only: 5.3×10^{10})
Seitzinger and Giblin [1996]	1.43×10^{12}
N Sources: N_2 Fixation, mol N yr⁻¹	
Michaels et al. [1996]	$3.7 – 6.4 \times 10^{12}$
Gruber and Sarmiento [1997]	2.3×10^{12}
Hansell et al. [2004]	0.3×10^{12}
Capone et al. [2005]	1.6×10^{12}
N Sources: Atmospheric Deposition, mol N yr⁻¹	
Nixon et al. [1996]	0.13×10^{12}
CO_2 Flux	
Model (this study)	0.18 Pg C yr⁻¹
	(MAB only: 4.2×10^{12} g C yr⁻¹)
Takahashi et al. [2002]	−0.6 Pg C yr⁻¹

are set to a small positive number. Analysis of our model results suggests this approach to work well. Boundary artifacts, in particular, elevated chlorophyll levels and elevated primary production, are limited to the immediate vicinity of open boundaries and do not affect the continental shelf area of the MAB.

[35] Further challenges in capturing continental shelf processes arise from the pronounced benthic-pelagic coupling and the input of nutrients and organic matter from land. In contrast to open ocean regions, steady state assumptions can hardly be made and benthic processes cannot be ignored. On the one hand, it becomes possible to assess the effects of variability on coastal ecosystems and elemental fluxes through the use of coupled models. On the other hand, model validation is difficult because there are few permanent features and the variability on sub-seasonal scales is dominated by sporadic events (e.g., wind-induced upwelling events and frontal shifts). We chose to compare climatological and regionally integrated means of surface chlorophyll, nutrients, primary production and denitrification, and statistical measures of pattern variability (the correlation and centered RMS difference of simulated and SeaWiFS chlorophyll).

[36] Denitrification in shelf sediment is known to be a quantitatively important sink in the global nitrogen cycle [*Hattori*, 1983; *Codispoti and Christensen*, 1985; *Christensen et al.*, 1987]. Our model suggests this flux to be important in reducing primary production on the shelf as well. Accurate prediction of sediment denitrification is hence crucial in simulating shelf production, but currently dependent on only few direct measurements. It would be costly to measure denitrification rates at high spatial and temporal resolution; hence, the development of well-constrained models (e.g., *Seitzinger and Giblin* [1996], *Middelburg et al.* [1996], and this study) may be more practical. Our model is based on *Seitzinger and Giblin*'s [1996] approximation of denitrification with sediment oxygen consumption, and our estimates hence hinge on the validity of this relationship.

[37] In our analysis, denitrification removes the majority of nitrogen entering the MAB in dissolved or particulate form, significantly more than enters from rivers, and thus makes the shelf system a net sink in the NA nitrogen cycle. This result is consistent with the observational-based estimates of *Seitzinger and Giblin* [1996], who suggested that denitrification on the NA shelves exceeds nitrogen inputs from land and must be sustained by fixed nitrogen that is imported from the open ocean. Assuming that the MAB shelf is representative of the NA shelves we can extrapolate the denitrification flux to the whole NA. Using the model-predicted mean denitrification flux for the MAB of 1.13 mmol N m^{-2} d^{-1} and a shelf area of 5.66×10^{12} m^2 [*Pilson and Seitzinger*, 1996] the extrapolation yields 2.3×10^{12} mol N yr^{-1}. Estimates of N$_2$ fixation for the NA vary by an order of magnitude (Table 2). Our denitrification estimate is 35% of the largest N$_2$ fixation estimate by *Michaels et al.* [1996], but 7 times higher than the most conservative estimate by *Hansell et al.* [2004]. Onwelling of inorganic nitrogen onto the continental shelves and subsequent denitrification are consequently key components of the NA nitrogen cycle,

emphasizing the need to better represent margin processes in basin-wide and global models.

[38] A large nitrogen sink on the continental shelves is likely to have implications for carbon cycling. Since the nitrogen import to the MAB is likely to be accompanied by an influx of inorganic carbon, the denitrification flux should be associated with an outgassing of CO$_2$. For the sake of simplicity we assume here that carbon and nitrogen import occur in Redfield ratio and can then estimate the outgassing of CO$_2$ at 0.19 PgC yr^{-1} (1 Pg = 10^{15}g) (Loss of fixed nitrogen from the North Atlantic shelf area determined as follows: 2.3×10^{12} mol N yr$^{-1} \times 106/16 = 15.2 \times 10^{12}$ mol C yr^{-1} multiplied by the molar mass of C (12 g) yields 0.18×10^{15} gC yr^{-1}). In comparison, *Takahashi et al.*'s [2002] estimate of the NA uptake of CO$_2$ is 0.6 PgC yr^{-1}. However, our estimate should not be mistaken for a carbon budget of the shelves. We did not address the transformation of river and estuarine dissolved organic matter, oxidation of which could result in an inorganic carbon source [*Borges and Frankignoulle*, 1999], and the possibility of inorganic carbon export through isopycnal export of CO$_2$-supersaturated shelf water in winter [*Tsunogai et al.*, 1999; *Yool and Fasham*, 2001].
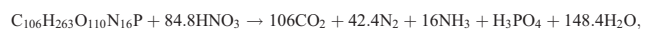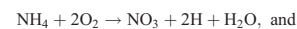
Appendix A: Biological Bottom Boundary Condition

[39] We assume that (1) all organic matter (large and small detritus, phytoplankton) is remineralized instantaneously upon reaching the bottom, (2) sediment oxygen is consumed only in the oxidation of carbon and the nitrification of ammonium to nitrate, (3) denitrification is related to sediment oxygen consumption according to

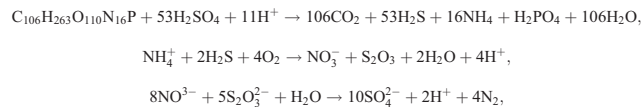$$\text{denitrification (mol N m}^{-2}\text{ d}^{-1}) = 0.105$$
$$* \text{ sediment oxygen consumption (mol O}_2\text{ m}^{-2}\text{ d}^{-1}), \quad (A1)$$

and (4) oxygenic mineralization, nitrification and denitrification follow

$$C_{106}H_{263}O_{110}N_{16}P + 106O_2 \leftrightarrow 106CO_2 + 16NH_4 + H_2PO_4 + 122H_2O,$$

$$NH_4 + 2O_2 \rightarrow NO_3 + 2H + H_2O, \text{ and}$$

$$C_{106}H_{263}O_{110}N_{16}P + 84.8HNO_3 \rightarrow 106CO_2 + 42.4N_2 + 16NH_3 + H_3PO_4 + 148.4H_2O,$$

respectively. Let $x \in [0,1]$ be the fraction of carbon oxidation that occurs through denitrification. In the mineralization of 1 mol of organic matter the sediment oxygen consumption amounts to $(1 - x) * 106 + x * 84.8 * 2 = 106 + 63.6 * x$ moles oxygen and the denitrified nitrogen amounts to $x * 84.8$ moles nitrogen. Substituting into equation (A1), $84.8x = 0.105 * (106 + 63.6x)$ yields $x = 0.14$. Hence 14% of organic matter is mineralized through denitrification, while 86% is oxidized directly. The net yield of ammonium from the mineralization of 1 mol of organic matter comprises $0.86*16 = 13.8$ mol NH$_4$ from direct carbon oxidation and $-0.14*84.8+0.14*16 = -9.6$ mol NH$_4$ consumed in coupled nitrification/denitrification, which amounts to a net yield of 4 mol NH$_4$ and 6 mol N$_2$.

[40] At a shallow, nearshore site in Long Island Sound, *Mackin and Swider* [1989] found sulfate reduction coupled with nitrification and sulfide oxidation to be the dominant pathway of organic matter decomposition (they found 3– 14% to be due to aerobic decomposition, 65–85% to be due to sulfate reduction and the rest due to coupled nitrification-denitrification). The sulfate reduction, nitrification and sulfide oxidation reactions follow

$$C_{106}H_{263}O_{110}N_{16}P + 53H_2SO_4 + 11H^+ \rightarrow 106CO_2 + 53H_2S + 16NH_4 + H_2PO_4 + 106H_2O,$$

$$NH_4^+ + 2H_2S + 4O_2 \rightarrow NO_3^- + S_2O_3 + 2H_2O + 4H^+,$$

$$8NO^{3-} + 5S_2O_3^{2-} + H_2O \rightarrow 10SO_4^{2-} + 2H^+ + 4N_2,$$

respectively [after *Mackin and Swider*, 1989; *Jørgensen*, 1996]. Assuming that 75% of organic matter is decomposed by sulfate reduction according to the above stoichiometries would result in at least 0.75*8 mol N_2 = 6 mol N_2 per mol of organic matter. Our estimate of 4 mol of NH4 and 6 mol of N_2 being returned for each mol of organic matter (derived above) is thus a conservative estimate of the amount of fixed nitrogen removed in sediment denitrification.

Appendix B: Taylor Diagram

[41] In the Taylor diagram [*Taylor*, 2001] the correlation coefficient R, the centered RMS error E, and the ratio of the standard deviations σ_n of a test field (typically a model simulated field p) and a reference field (typically an observed field q) are displayed by the location of one point (representing the test field) in relation to the reference point (representing the reference field). The correlation coefficient measures the centered pattern agreement of the variations of the two fields regardless of amplitude; in other words, correlation is high ($R{\rightarrow}1$) if the test field is correctly phased. The centered RMS error measures the difference between the fields with the overall bias removed, but this index by itself can not reveal if the RMS error is due to differences in the phasing or in the amplitude of variations. The ratio of the standard deviations indicates if the test field overestimated ($\sigma_n > 1$) or underestimated ($\sigma_n < 1$) the amplitude of variations. The reference point is located on the x axis at $\sigma_n = 1$ (see, for example, Figure 8). The radial distance of the test point from the origin indicates the normalized standard deviation ($\sigma_n = \sigma_p/\sigma_q$), its azimuthal position indicates the correlation coefficient, and its distance from the reference point indicates the centered RMS error. In our case of comparing surface chlorophyll fields we follow *Lima and Doney* [2004] in defining total space-time, spatial-annual and spatial-monthly statistics.

References

Aller, R. C. (1980), Diagenetic processes near the sediment-water interface of Long Island Sound: I. Decomposition and nutrient element chemistry (S, N, P), *Adv. Geophys.*, 22, 238–250.

Andersen, V., P. Nival, and R. P. Harris (1987), Modelling of a planktonic ecosystem in an enclosed water column, *J. Mar. Biol. Assoc. U. K.*, 67, 407–430.

Antoine, D., J. M. Andre, and A. Morel (1996), Oceanic primary production: 2. Estimation at global scale from satellite (coastal zone color scanner) chlorophyll, *Global Biogeochem. Cycles*, 10, 57–69.

Behrenfeld, M. J., and P. G. Falkowski (1997), Photosynthetic rates derived from satellite-based chlorophyll concentration, *Limnol. Oceanogr.*, 42, 1–20.

Biscaye, P. E., C. N. Flagg, and P. G. Falkowski (1994), The shelf edge exchange processes experiment, SEEP-II: An introduction to hypotheses, results and conclusions, *Deep Sea Res., Part II*, 41, 231–252.

Borges, A. V., and M. Frankignoulle (1999), Daily and seasonal variations of the partial pressure of CO_2 in surface seawater along Belgian and southern Dutch coastal areas, *J. Mar. Syst.*, 19, 251–266.

Brown, W. S. (1984), A comparison of Georges Bank, Gulf of Maine, and New England Shelf tidal dynamics, *J. Phys. Oceanogr.*, 14, 145–167.

Capone, D. G., J. A. Burns, J. P. Montoya, A. Subramaniam, C. Mahaffey, T. Gunderson, A. F. Michaels, and E. J. Carpenter (2005), Nitrogen fixation by *Trichodesmium* spp.: An important source of new nitrogen to the tropical and subtropical North Atlantic Ocean, *Global Biogeochem. Cycles*, 19, GB2024, doi:10.1029/2004GB002331.

Chapman, D. C. (1985), Numerical treatment of cross-shelf open boundaries in a barotropic coastal ocean model, *J. Phys. Oceanogr.*, 15, 713–748.

Chapman, D. C., and R. C. Beardsley (1989), On the origin of shelf water in the Middle Atlantic Bight, *J. Phys. Oceanogr.*, 19, 384–391.

Chen, C., and R. C. Beardsley (1998), Tidal mixing over a finite amplitude asymmetric bank: A model study with application to Georges Bank, *J. Mar. Res.*, 56, 1163–1201.

Christensen, J. P. (1994), Carbon export from continental shelves, denitrification and atmospheric carbon dioxide, *Cont. Shelf Res.*, 14, 547–576.

Christensen, J. P., J. W. Murray, A. H. Devol, and L. A. Codispoti (1987), Denitrification in continental shelf sediments has major impact on the oceanic nitrogen budget, *Global Biogeochem. Cycles*, 1, 97–116.

Codispoti, L. A., and J. P. Christensen (1985), Nitrification, denitrification, nitrous oxide cycling in the eastern tropical South Pacific Ocean, *Mar. Chem.*, 16, 277–300.

Codispoti, L. A., J. A. Brandes, J. P. Christensen, A. H. Devol, S. W. A. Naqvi, H. W. Paerl, and T. Yoshinari (2001), The oceanic fixed nitrogen and nitrous oxide budgets: Moving targets as we enter the anthropocene?, *Sci. Mar.*, 65, 85–105.

Devol, A. H. (1991), Direct measurement of nitrogen gas fluxes from continental shelf sediments, *Nature*, 349, 319–321.

Devol, A. H., and J. P. Christensen (1993), Benthic fluxes and nitrogen cycling in sediments of the continental margin of the eastern North Pacific, *J. Mar. Res.*, 51, 345–372.

Eppley, R. W. (1972), Temperature and phytoplankton growth in the sea, *Fish. Bull.*, 70, 1063–1085.

Evans, G. T., and J. S. Parslow (1985), A model of annual plankton cycles, *Biol. Oceanogr.*, 3, 327–347.

Falkowski, P. G. (1980), Light-shade adaptation in marine phytoplankton, in *Primary Productivity in the Sea*, edited by P. G. Falkowski, pp. 99–119, Springer, New York.

Falkowski, P. G., C. N. Flagg, G. T. Rowe, S. L. Smith, T. E. Whitledge, and C. D. Wirick (1988), The fate of a spring diatom bloom: Export or oxidation?, *Cont. Shelf Res.*, 8, 457–484.

Fasham, M. J. R. (1995), Variations in the seasonal cycle of biological production in subarctic oceans: A model sensitivity analysis, *Deep Sea Res., Part I*, 42, 1111–1149.

Fasham, M. J. R., H. W. Ducklow, and S. M. McKelvie (1990), A nitrogen-based model of plankton dynamics in the oceanic mixed layer, *J. Mar. Res.*, 48, 591–639.

Fennel, K., M. Losch, J. Schroter, and M. Wenzel (2001), Testing a marine ecosystem model: Sensitivity analysis and parameter optimization, *J. Mar. Syst.*, 28, 45–63.

Flather, R. A. (1976), A tidal model of the northwest European continental shelf, *Mem. Soc. R. Sci. Liege*, 6, 141–164.

Franks, P. S. J., and C. Chen (1996), Plankton production in tidal fronts: A model of Georges Bank in summer, *J. Mar. Res.*, 54, 631–651.

Garrett, C. J. (1972), Tidal response of the Bay of Fundy and Gulf of Maine, *Nature*, 238, 441–443.

Geider, R. J., H. L. McIntyre, and T. M. Kana (1996), A dynamic model of photoadaptation in phytoplankton, *Limnol. Oceanogr.*, 41, 1–15.

Geider, R. J., H. L. McIntyre, and T. M. Kana (1997), Dynamic model of phytoplankton growth and acclimation: Responses of the balanced growth rate and the chlorophyll a: Carbon ratio to light, nutrient-limitation and temperature, *Mar. Ecol. Prog. Ser.*, 148, 187–200.

Gentleman, W., A. Leising, B. Frost, S. Strom, and J. Murray (2003), Functional responses for zooplankton feeding on multiple resources: A review of assumption and biological dynamics, *Deep Sea Res., Part II*, 50, 2847–2876.

Giblin, A. E., C. S. Hopkinson, J. Tucker, B. L. Nowicki, and J. R. Kelly (1994), Metabolism, nutrient cycling and denitrification in Boston Harbor and Massachusetts Bay sediments in 1993, *Environ. Qual. Tech. Rep. 94*, 54 pp., Mass. Water Resour. Auth., Boston.

Gruber, N., and J. L. Sarmiento (1997), Global patterns of marine nitrogen fixation and denitrification, *Global Biogeochem. Cycles*, 11, 235–266.

Haidvogel, D. B., H. Arango, K. Hedstrom, A. Beckmann, P. Rizzoli, and A. Shchepetkin (2000), Model evaluation experiments in the North Atlantic Basin: Simulations in non-linear terrain-following coordinates, *Dyn. Atmos. Oceans*, 32, 239–281.

Hansell, D. A., N. R. Bates, and D. B. Olson (2004), Excess nitrate and nitrogen fixation in the North Atlantic Ocean, *Mar. Chem.*, 84, 243–265.

Hattori, A. (1983), Denitrification and dissimilatory nitrate reduction, in *Nitrogen in the Marine Environment*, edited by E. J. Carpenter and D. G. Capone, pp. 191–232, Elsevier, New York.

Hedges, J. I., and R. G. Keil (1995), Sedimentary organic preservation: An assessment and speculative synthesis, *Mar. Chem.*, 49, 81–115.

Hopkinson, C. R., R. D. Fallon, B.-O. Jansson, and J. P. Shubauer (1991), Community metabolism and nutrient cycling at Gray's Reef, a hard bottom habitat in the Georgia Bight, *Mar. Ecol. Prog. Ser.*, 73, 105–120.

Jensen, M. H., E. Lomstein, and J. Sorensen (1990), Benthic NH_4^+ and NO_3^- flux following sedimentation of a spring phytoplankton bloom in Aarhus Bight, Denmark, *Mar. Ecol. Prog. Ser.*, 61, 87–96.

Jørgensen, B. B. (1996), Material flux in the sediment, in *Eutrophication in Coastal Marine Ecosystems, Coastal Estuarine Stud.*, vol. 52, edited by B. B. Jørgensen and K. Richardson, pp. 115–135, AGU, Washington, D. C.

Kelly, J. R., and B. L. Nowicki (1993), Direct measurements of denitrification in Boston Harbor and Massachusetts Bay sediments, *Environ. Qual. Tech. Rep. 93*, 321 pp., Mass. Water Resour. Auth., Boston.

Kirk, J. T. O. (1983), *Light and Photosynthesis in Aquatic Ecosystems*, Cambridge Univ. Press, New York.

Laursen, A. E., and S. P. Seitzinger (2002), The role of denitrification in nitrogen removal and carbon mineralization in Mid-Atlantic Bight sediments, *Cont. Shelf Res.*, 22, 1397–1416.

Laws, E. A., and T. T. Bannister (1980), Nutrient- and light-limited growth of Thalassiosira fluviatis in conditions of continuous culture, with implications for phytoplankton growth in the ocean, *Limnol. Oceanogr.*, 25, 457–473.

Leonard, C. L., C. R. McClain, R. Murtugudde, E. E. Hofmann, and L. W. Harding (1999), An iron-based ecosystem model of the central equatorial Pacific, *J. Geophys. Res.*, 104, 1325–1341.

Lima, I. D., and S. C. Doney (2004), A three-dimensional, multi-nutrient and size-structured ecosystem model for the North Atlantic, *Global Biogeochem. Cycles*, 18, GB3019, doi:10.1029/2003GB002146.

Lohse, L., J. F. P. Malschaert, C. P. Slomp, W. Helder, and W. V. Raaphorst (1993), Nitrogen cycling in North Sea sediments: Interaction of denitrification and nitrification in offshore and coastal areas, *Mar. Ecol. Prog. Ser.*, 101, 283–296.

Longhurst, A., S. Sathyendranath, T. Platt, and C. Caverhill (1995), An estimate of global primary production in the ocean from satellite radiometer data, *J. Plankton Res.*, 17, 1245–1271.

Lynch, D. R., and C. E. Naimie (1993), The M2 tide and its residual on the outer banks of the Gulf of Maine, *J. Phys. Oceanogr.*, 23, 2222–2253.

Mackin, J. E., and K. T. Swider (1989), Organic matter decomposition pathways and oxygen consumption in coastal marine sediments, *J. Mar. Syst.*, 47, 681–716.

Malanotte-Rizzoli, P., K. Hedstrom, H. Arango, and D. B. Haidvogel (2000), Water mass pathways between the subtropical and tropical ocean in a climatological simulation of the North Atlantic Ocean circulation, *Dyn. Atmos. Oceans*, 32, 209–237.

Malone, T. C., T. S. Hopkins, P. G. Falkowski, and T. E. Whitledge (1983), Production and transport of phytoplankton biomass over the continental shelf of the New York Bight, *Cont. Shelf Res.*, 1, 305–337.

Michaels, A. F., D. Olson, J. L. Sarmiento, J. W. Ammerman, K. Fanning, R. Jahnke, A. H. Knap, F. Lipschultz, and J. M. Prospero (1996), Inputs, losses and transformations of nitrogen and phosphorus in the pelagic North Atlantic, in *Nitrogen Cycling in the North Atlantic Ocean and Its Watersheds*, edited by R. W. Howarth, pp. 181–226, Springer, New York.

Middelburg, J. J., and K. Soetaert (2004), The role of sediments in shelf ecosystem dynamics, in *The Sea*, vol. 13, edited by A. R. Robinson and K. Brink, pp. 353–373, Harvard Univ. Press, Cambridge, Mass.

Middelburg, J. J., K. Soetaert, P. M. J. Herman, and C. Heip (1996), Denitrification in marine sediments: A model study, *Global Biogeochem. Cycles*, 10, 661–673.

Moody, J. A., et al. (1984), Atlas of tidal elevation and current observations on the Northeast American Continental Shelf and Slope, *U.S. Geol. Surv. Bull.*, 1611, 122 pp.

Moskilde, E. (1996), *Topics in Non-Linear Dynamics: Application to Physics, Biology and Economic Systems*, World Sci., Hackensack, N. J.

Nixon, S. W., and M. E. Q. Pilson (1983), Nitrogen in estuarine and coastal marine ecosystems, in *Nitrogen in the Marine Environment*, edited by E. J. Carpenter and D. G. Capone, pp. 565–648, Elsevier, New York.

Nixon, S. W., C. A. Oviatt, and S. S. Hale (1976), Nitrogen regeneration and the metabolism of coastal marine bottom communities, in *The Role of Terrestrial and Aquatic Organism Decomposition Processes*, edited by J. M. Anderson and A. Macfadyen, pp. 269–283, Blackwell Sci., Malden, Mass.

Nixon, S. W., et al. (1996), The fate of nitrogen and phosphorus at the land-sea margin of the North Atlantic, *Biogeochemistry*, 35, 141–180.

Olson, R. J. (1981), Differential photoinhibition of marine nitrifying bacteria: A possible mechanism for the formation of the primary nitrite maximum, *J. Mar. Res.*, 39, 227–238.

O'Reilly, J. E., and D. A. Busch (1984), Phytoplankton primary production on the northwestern Atlantic shelf, *Rapp. P.V. Reun. Cons. Int. Explor. Mer*, 183, 255–268.

O'Reilly, J. E., and C. Zetlin (1998), Seasonal, horizontal, and vertical distribution of phytoplankton chlorophyll a in the northeast US continental shelf ecosystem, report, U.S. Dep. of Commer., Seattle, Wash.

O'Reilly, J. E., C. Evans-Zetlin, and D. A. Busch (1987), Primary production, in *Georges Bank*, edited by R.H. Backus, pp. 220–233, MIT Press, Cambridge, Mass.

Oschlies, A., and V. Garcon (1999), An eddy-permitting coupled physical-biological models of the North Atlantic: 1. Sensitivity to advection numerics and mixed layer, *Global Biogeochem. Cycles*, 13, 135–160.

Parker, R. A. (1993), Dynamic models for ammonium inhibition of nitrate uptake by phytoplankton, *Ecol. Modell.*, 66, 113–120.

Pilson, M. E. Q., and S. P. Seitzinger (1996), Areas of shallow water in the North Atlantic, *Biogeochemistry*, 35, 227–233.

Premuzic, E. T., C. M. Benkovitz, J. S. Gaffney, and J. J. Walsh (1982), The nature and distribution of organic matter in the surface sediments of world oceans and seas, *Org. Geochem.*, 4, 63–77.

Raaphorst, W. V., H. T. Kloosterhuis, A. Cramer, and K. J. M. Bakker (1990), Nutrient early diagenesis in the sandy sediments of the Dogger Bank area, North Sea: Pore water results, *Neth. J. Sea Res.*, 26, 25–52.

Rowe, G. T., C. H. Clifford, and K. L. J. Smith (1977), Nutrient regeneration in sediments off Cape Blanc, *Spanish Sahara, Deep Sea Res.*, 24, 57–63.

Sakshaug, E., K. Andresen, and D. A. Kiefer (1989), A steady state description of growth and light absorption in the marine planktonic diatom Skeletonema costatum, *Limnol. Oceanogr.*, 34, 198–205.

Seitzinger, S. P., and A. E. Giblin (1996), Estimating denitrification in North Atlantic continental shelf sediments, *Biogeochemistry*, 35, 235–260.

Shchepetkin, A. F., and J. C. McWilliams (2005), The Regional Ocean Modeling System: A split-explicit, free-surface, topography following coordinates ocean model, *Ocean Modell.*, 9, 347–404.

Smith, S., and F. MacKenzie (1987), The ocean as a net heterotrophic system: Implications for the carbon biogeochemical cycle, *Global Biogeochem. Cycles*, 1, 187–198.

Soetaert, K., J. J. Middelburg, P. M. J. Herman, and K. Buis (2000), On the coupling of benthic and pelagic biogeochemical models, *Earth Sci. Rev.*, 51, 173–201.

Takahashi, T., et al. (2002), Global sea–air CO_2 flux based on climatological surface ocean pCO_2, and seasonal biological and temperature effects, *Deep Sea Res., Part II*, 49, 1601–1622.

Taylor, A. H. (1988), Characteristic properties of models for the vertical distribution of phytoplankton under stratification, *Ecol. Modell.*, 40, 175–199.

Taylor, A. H., A. J. Watson, M. Ainsworth, J. E. Robertson, and D. R. Turner (1991), A modelling investigation of the role of phytoplankton in the balance of carbon at the surface of the North Atlantic, *Global Biogeochem. Cycles*, 5, 151–171.

Taylor, K. E. (2001), Summarizing multiple aspects of model performance in a single diagram, *J. Geophys. Res.*, *106*(D7), 7183–7192.

Tsunogai, S., S. Watanabe, and T. Sato (1999), Is there a "continental shelf pump" for the absorption of atmospheric CO_2?, *Tellus, Ser. B*, *51*, 701–712.

Verity, P. G., J. E. Bauer, C. N. Flagg, D. J. DeMaster, and D. J. Repeta (2002), The Ocean Margins Program: An interdisciplinary study of carbon sources, transformations, and sinks in a temperate continental margin system, *Deep Sea Res., Part II*, *49*, 4273–4295.

Walsh, J., G. Rowe, R. Iverson, and C. McRoy (1981), Biological export of shelf carbon is a sink of the global CO_2 cycle, *Nature*, *292*, 196–201.

Walsh, J., P. Biscaye, and G. Csanady (1988), The 1983–1984 Shelf Edge Exchange Processes (SEEP)-I experiment: Hypotheses and highlights, *Cont. Shelf Res.*, *8*, 435–456.

Wroblewski, J. S. (1989), A model of the spring bloom in the North Atlantic and its impact on ocean optics, *Limnol. Oceanogr.*, *34*, 1563–1571.

Yool, A., and M. J. R. Fasham (2001), An examination of the "continental shelf pump" in an open ocean general circulation model, *Global Biogeochem. Cycles*, *15*, 831–844.

————————————

K. Fennel, D. Haidvogel, J. Levin, and J. Wilkin, Institute for Marine and Coastal Sciences, Rutgers University, 71 Dudley Road, New Brunswick, NJ 08901, USA. (kfennel@marine.rutgers.edu; dale@marine.rutgers.edu; julia@marine.rutgers.edu; wilkin@marine.rutgers.edu)

J. Moisan, Laboratory for Hydrospheric Processes, Observation Science Branch, NASA Goddard Space Flight Center, Wallops Flight Facility, Wallops Island, VA 23337, USA. (jmoisan@osb.wff.nasa.gov)

J. O'Reilly, NOAA National Marine Fisheries Service Narragansett Laboratory, 28 Tarzwell Drive, Narragansett, RI 02882, USA. (jay.o'reilly@noaa.gov)